Oxide Surface Structure Determination 4.0:

IrO_2 Surface Complexions Identified Through

Machine Learning and Surface Investigations

*Jakob Timmermann[1], Florian Kraushofer[2], Nikolaus Resch[2], Peigang Li[3], Yu Wang[4], Zhiqiang Mao[3,4], Michele Riva[2], Yonghyuk Lee[1], Carsten Staacke[1], Michael Schmid[2], Christoph Scheurer[1], Gareth S. Parkinson[2], Ulrike Diebold[2], and Karsten Reuter[1,5,]**

[1]Chair for Theoretical Chemistry and Catalysis Research Center
Technical University of Munich, Lichtenbergstr. 4, D-85747 Garching (Germany)

[2]Institute of Applied Physics, Technical University of Vienna,
Wiedner Hauptstr. 8-10/134, A-1040 Vienna (Austria)

[3]Department of Physics and Engineering Physics, Tulane University,
New Orleans, LA 70118 (USA)

[4]Department of Physics, The Pennsylvania State University,
University Park, PA 16803 (USA)

[5]Fritz-Haber-Institut der Max-Planck-Gesellschaft,
Faradayweg 4-6, D-14195 Berlin (Germany)

*corresponding author: karsten.reuter@ch.tum.de

Abstract: We train a Gaussian Approximation Potential (GAP) with density-functional theory data to enable predictive-quality global geometry optimization of low-index rutile IrO_2 facets through

simulated annealing. *Ab initio* thermodynamics identifies novel (101) and (111) (1×1)-terminations competitive with (110) in reducing environments. Electron backscatter diffraction experiments (EBSD) on macroscopic single crystals show that the (101) facets indeed dominate, and both low energy electron diffraction (LEED) and scanning tunneling microscopy (STM) images reveal their (1×1) periodicity. X-ray photoelectron spectroscopy (XPS) experiments show significantly reduced Ir in the surface, with a binding energy shift consistent with theoretical predictions for the new (101) termination. These new terminations can be seen as a thin reduced interphase atop the IrO_2 substrate, fully analogous to the surface and interfacial complexions discussed in the context of complex ceramic battery materials.

Keywords: Machine Learned Potentials, Rutile Oxides, Global Geometry Optimization, Complexions, Scanning Tunneling Microscopy, X-ray Photoelectron Spectroscopy

Over the last two decades, first-principles electronic structure theory calculations based on density-functional theory (DFT) have become a standard tool in surface structure determination, which is an essential step to establish the structure/reactivity relationship at surfaces and interfaces. In the canonical approach, local geometry optimization of a set of trial structures identifies minima on the ground-state potential energy surface (PES). For the structure of the energetically lowest minimum, observables are then computed to check for consistency with available signatures from experiment, typically scanning-probe or spectroscopic data. Accepting some uncertainty in the approximate DFT energetics, this last step can also be extended to the structures of a number of lowest-energy minima. Finally, depending on its energetics and consistency with experiment, one structure is declared to be the best. While immensely successful, the fundamental limitation of this

approach lies in its dependence on the initially chosen set of trial structures. The risk of missing the truly relevant (energetically lowest-lying) PES minimum is clear.

With increasing numerical efficiency of DFT calculations and available computational power, DFT-based global geometry optimization has been heralded as a significant step to overcome this limitation.[1-5] Despite impressive successes of, e.g., first-principles simulated annealing or basin hopping work, it is probably fair to say that this direct approach has never truly affected the popularity of the 'trial set and local geometry optimization' approach to surface structure determination. The excessive number of total energy evaluations required by even the most efficient global optimization algorithms[6, 7] leads quickly to an intractable computational demand, particularly for reconstructions with large surface unit cells. Fortunately, machine-learned (ML) interatomic potentials[8, 9] may now overcome this deadlock and enable a "surface structure determination 4.0", i.e. a paradigm shift towards automatic structure searches way beyond what was possible so far. These potentials can be trained with a feasible number of DFT calculations or, if needed, can be retrained on-the-fly in the course of an ongoing global geometry optimization. Crucially, the optimization itself is performed with the numerically non-intense ML potential, which enables extensive sampling of the configuration space.

Here, we exemplify the prospects of this concept by identifying hitherto unknown and in their simplicity completely unexpected surface terminations of rutile-structured oxides. The original motivation to search for corresponding structures came from the recent emphasis on so-called complexions in the context of ceramic battery materials.[10] Such complexions correspond to surface (or interfacial) phases that possess thermodynamically-determined equilibrium thicknesses on the order of nanometers, but are neither merely thin versions of known 3D bulk phases, nor just a reconstructed surface layer. Following recent empirical indications that IrO_2 catalysts for proton-

exchange membrane (PEM) water electrolysis with increased activity and sufficient stability can be prepared by electrochemical activation with a small number of reductive formation cycles,[11, 12] we hypothesized that this might create a hitherto unknown metal-rich complexion even on this comparably simple metallic oxide that could act as a structurally stable alternative to the so-called hydrous oxides which are commonly considered to be too unstable for technical use. After training a ML Gaussian Approximation Potential (GAP)[13, 14] with DFT data, simulated-annealing-based global optimization runs indeed immediately lead to very stable new terminations on the (101) and (111) low-index surfaces of rutile IrO_2. Intriguingly, these complexions are neither delicate amorphous films, nor complex, large-unit-cell reconstructions. Instead, they can simply be seen as a reordering of the stacking in the top atomic layers. Direct *ab initio* thermodynamics[15] calculations confirm the high stability of these novel complexions under strongly reducing conditions close to the phase separation into metallic Ir and oxygen[16] – not only on IrO_2, but also on RuO_2, which is the alternative state-of-the-art rutile-structured catalyst used in PEM electrolysis. The theoretical predictions are supported by surface investigations of IrO_2 single crystals grown using a chemical vapor transport method. These crystals indeed exhibit (101) facets rather than the more frequently studied low-energy (110) orientation of rutile.[17, 18] Characterization by low-energy electron diffraction (LEED), scanning-tunneling microscopy (STM) and X-ray photoelectron spectroscopy (XPS) confirms the properties of the predicted metal-rich complexions, explaining why IrO_2 nanoparticles often expose (101) facets.[19-25]

Our investigation starts with the creation of a reference database of DFT structures to train the non-parametric GAP potential. GAPs decompose the total energy of a system into a sum of atomic energies that depend on the local chemical environment.[13, 14] This dependence is learned from the atomic environments present in the reference database through Gaussian process regression. For

energy predictions, the similarity between each atom in an unknown structure and representative training atoms is then determined via a kernel function. In this work, we employ the smooth overlap of atomic positions (SOAP) kernel,[26] which considers all neighboring atoms within a radius of 5.5 Å, combined with a simple two-body kernel based on interatomic distances. The reference database comprises 136 structures calculated with QuantumEspresso[27] and the RPBE[28] exchange-correlation functional. For an efficient training, these structures span a range of most diverse chemical environments. As further detailed in the supporting information (SI), they comprise various optimized or near-optimum crystalline bulk and low-index surface geometries of different stoichiometry, as well as highly non-equilibrium structures taken from snapshots of high-temperature molecular dynamics (MD) simulations of differently shaped and sized nanoparticles. Validated against an equally diverse set of 39 structures not used in the training, the final GAP reproduces the widely varying DFT formation energies with a mean average error of 25 meV/atom.

In order to explore a possible formation of complexions, we can now exploit the low computational demand of the GAP potential and perform extensive simulated annealing MD runs for all five symmetry-inequivalent low-index surfaces[29] of rutile IrO_2, each time starting with the metal-rich regular (1×1) termination expected for reducing conditions close to the decomposition of the oxide. Specifically, we employ periodic boundary condition supercells with thick slabs comprising at least seven rutile trilayers and (3×3) or (4×4) surface unit cells as further detailed in the SI. The temperature is initially raised to around 1000 K and held there for 20 ps, before a slow cooling rate of 3 K/ps is applied during an additional 250 ps. After a final geometry optimization, we obtain new structures with a significantly lower energy, in particular for the (101) [or the symmetry-equivalent (011)] and the (111) orientations, cf. SI. Analysis of these structures shown

in **Figure 1** intriguingly reveals that neither corresponds to a reconstruction with a lowered translational symmetry, but is instead a reordering of the original rutile layering sequence that preserves the regular (1×1) lateral periodicity. Direct recalculation and geometry re-optimization of these structures at the DFT RPBE level confirms the reliability of the GAP prediction. The structures are stable PES minima that are significantly lower in energy than the regular Ir-rich (1×1) termination for the respective orientation. In fact, the metastability of e.g. the regular Ir-rich (101) termination in DFT calculations appears to be only an artefact of conventionally employed slab thicknesses that typically only allow a small number of surface layers to relax. For extended slabs where at least the five topmost layers are allowed to move, the regular Ir-rich termination relaxes barrierless into the new complexion even in laterally most restrictive (1×1) surface unit cells.

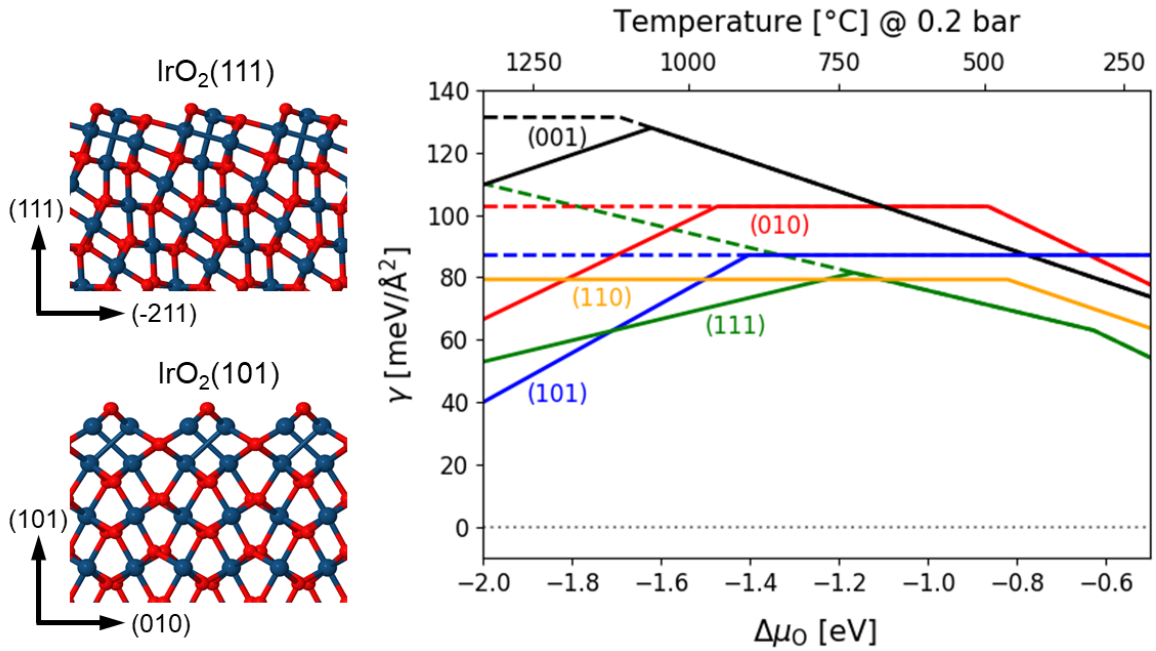

Figure 1: (Left) Side views of identified complexions. Ir and O atoms are drawn as blue (large) and red (small) spheres, respectively. (Right) Computed surface free energies γ of the five symmetry-inequivalent low-index facets in a pure oxygen atmosphere. In the top x axis, the

dependence on the oxygen chemical potential $\Delta\mu_O$ is translated into a temperature scale at 0.2 bar pressure, which corresponds to the oxygen partial pressure in air. The dashed lines indicate the surface free energies as would be obtained without consideration of the new complexions.

Within an *ab initio* thermodynamics framework[15] we can set the stability of these new structures into the context of all other possible and known (1×1) terminations of rutile IrO_2. Generally, there is at least one metal-rich, one stoichiometric and one oxygen-rich termination for each low-index facet, with some facets lacking some terminations and some facets additionally allowing e.g. for an oxygen-superrich termination as further detailed in Figs. S7-S11 in the SI.[30] Figure 1 shows the resulting surface phase diagram in an oxygen atmosphere, where only the lowest surface free energy is shown for each facet as a function of the chemical potential of oxygen $\Delta\mu_O$, as determined by the surrounding gas phase (see also SI). A kink in the surface free energy line reflects a change in the most stable termination, with metal-rich terminations exhibiting a positive slope, O-rich terminations a negative slope, and stoichiometric terminations being independent of $\Delta\mu_O$. For low oxygen chemical potentials, the complexions indeed lead to a significant lowering of the surface free energy. Thus, they do not only result as most stable terminations at reducing conditions, but also change the relative energetic ordering among the five low-index facets. This result seems robust with respect to the approximate DFT functional employed as we obtain essentially the same form and relative ordering of the surface free energies when computing them with the stronger-binding PBE[31] functional. What changes, though, are the absolute chemical potentials, i.e. the entire phase diagram shifts to lower $\Delta\mu_O$ (see Fig. S13). While we can therefore not fully quantify the exact gas-phase conditions of the phase stability limits, it is clear from Figure **1** that without the new complexions, the (110) facet would clearly be the lowest-energy orientation in reducing environments, in line with the predominant focus of any detailed surface science work in the last

decades on this particular facet of rutile-type crystals.[17, 18] Instead, the high stability of the complexions now makes the so far essentially disregarded (101) and (111) facets energetically competitive.

In order to test this surprising finding, we investigate the surfaces of IrO_2 single crystals. The crystals were grown in a tube furnace with an O_2 inflow of 100 ml/min at atmospheric pressure. Ir was supplied from Ir powder (99.99%) kept at 1250 °C, and condensation of the resulting IrO_3 gas led to the formation of flake-shaped IrO_2 crystals at 1000 °C at the colder end of the furnace. Two of the larger crystallites (both ca. 3 mm^2 top surface area) were chosen for surface studies. Electron backscatter diffraction (EBSD) immediately reveals that all areas where a diffraction pattern could be identified expose (101)-type surfaces, as shown in Fig. S18.

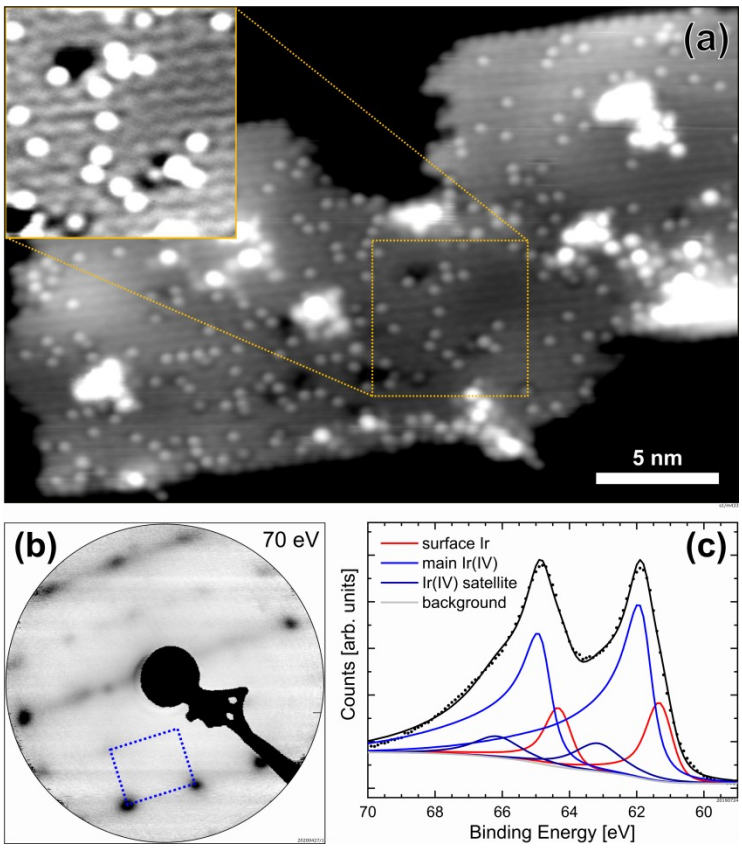

Figure 2: IrO_2 crystal after UHV preparation. (a) STM image of the IrO_2 sample (30 × 20 nm^2, $U_{sample} = -2$ V, $I_{tunnel} = 0.2$ nA), with the inset processed to enhance the visibility of the atomic

corrugation. STM is shown as taken, without correction for scanner drift. (b) LEED pattern of one of the IrO_2 crystals at 70 eV electron beam energy. A rectangular pattern (unit cell drawn in blue) is clearly visible, and its diffraction spots move towards the center of the screen with increasing energy, as expected for normal beam incidence. (c) XPS data (points) and fit (lines) of the Ir 4*f* region (Mg Kα anode).

The two IrO_2 samples were then loaded to an ultra-high vacuum (UHV) chamber and prepared by sputtering (1 keV Ar^+ ions, $p_{Ar} = 8 \times 10^{-6}$ mbar, 10 min) and annealing in oxygen (450 °C, 40 min). Oxygen gas was dosed on the sample through an oxygen shower, with the gas outlet very close to the sample. This increases the local pressure by a factor of ≈10–20 compared to the O_2 pressure measured in the chamber (5×10^{-6} mbar).

Low energy electron diffraction (LEED) images (**Figure 2**b and Figure S20) reveal a rectangular pattern with the spots moving towards the center of the screen with increasing incident beam energy. The unit cell size of $(0.58 \pm 0.04) \times (0.47 \pm 0.04)$ nm^2 was quantified using LEED patterns of a Pd(111) single crystal as a reference. These numbers are in good agreement with the (1×1) unit cell of IrO_2(101) (0.55×0.45 nm^2). Some additional diffraction spots are also observed, but these move in non-radial directions with increasing energy, indicating the presence of other facets for which the beam incidence is off-normal.

STM images acquired at room temperature after UHV preparation (**Figure 2**a) exhibit a zig-zag pattern with (1×1) symmetry. Since the intrinsic drift of the STM scanner cannot be corrected by comparison to a known structure, distance measurements are unreliable, but the 0.55×0.45 nm^2 spacing expected for an IrO_2(101)-(1×1) unit cell fits the data within the expected error. Some bright point features are also visible, which we attribute to either lattice defects or adsorbates.

Analysis of these features' positions (Figure S22) provides additional evidence that the STM image indeed shows the complexion, since they have a periodicity that would not be in agreement with a bulk-truncated (1×1) surface.

On one of the samples, a second, pseudo-hexagonal surface phase was also observed (Fig. S19). The nearest-neighbor distances were determined as ≈0.55 nm, which would fit an IrO_2(111)-(1×1) unit cell. However, since the unit cell angle cannot be accurately determined by STM alone, a (2×2) superstructure on Ir(111) could, in principle, also fit the data. We also note that a hexagonal reconstruction of the (101) facet was previously observed on rutile TiO_2(101),[32] and attributed to contamination.

XPS of the Ir 4*f* region is shown in **Figure 2**c. We fit the spectrum using peak shapes and oxide satellite peak positions from ref. [33], which results in a peak at 61.9 eV (blue) due to Ir(IV), and a lower-binding-energy component shifted by 0.6 eV at 61.3 eV (red). This is in excellent agreement with our initial-state calculations of the 4*f* DFT Kohn-Sham orbital positions for the IrO_2(101) complexion, which robustly yield an initial-state shift of 0.6 eV for the top two Ir layers with respect to a bulk-like Ir in the middle of the slab using both the RPBE and PBE functionals (see SI). A much larger shift (1.1 eV towards lower binding energies) is predicted for the top layer of the regular Ir-rich (101) termination. For comparison, we also acquired Ir 4*f* peak data from a freshly sputtered sample (Fig. S21), which is dominated by a strong contribution of metallic surface iridium at 60.9 eV, in agreement with the position reported in the literature for Ir single crystals.[31]

Overall, the experimental evidence clearly shows that the crystals are dominated by (101) facets with a (1×1) surface symmetry. Since the crystal growth direction was not enforced in any way, and the relatively rough, often vicinal surfaces would easily have allowed faceting to a more stable

orientation, the dominance of (101) surfaces is an indirect proof of their thermodynamic stability at the growth conditions, as predicted by theory. The LEED pattern, STM images and XPS analysis further support the predicted complexed IrO_2(101)-(1×1) surface, and motivate viewing the complexions as two layers with mixed Ir–O and Ir–Ir bonding atop the IrO_2 substrate, capped by oxygen. They are thus essentially surface precursors to a full reduction of the bulk oxide, and it is a peculiarity of the (101) and (111) orientations that this can be achieved through a mere reordering of the rutile layering sequence. This simultaneously allows to increase the coordination of the topmost Ir atoms (from 3-fold to 4-fold) and thereby stabilizes these structures. Adding further equivalent complexion layers does not further increase this coordination, and we correspondingly calculate higher surface free energies for such structures (see Fig. S12). As such, the identified complexions are indeed novel 2D interphases and not just thin versions of known 3D bulk structures. Representing precursors to a full reduction of the oxide, they are thus quite analogous to the much discussed surface oxides as precursors to a full oxidation of transition metals.[34-36]

With this understanding, one would expect such complexions to be a more general feature of oxides in reducing environments and in particular of rutile-structured oxides *per se*. Indeed, we compute a similar stability also for rutile RuO_2, where the complexions then equally render the (101) and (111) facets energetically competitive under reducing conditions as shown in Figure S14. For rutile TiO_2(101), no complexion is observed, but the observed (2×1) reconstruction also originates simply from a rearrangement of the surface layer.[37] This generality and simultaneous simplicity is, in our view, the most striking aspect of our findings. Protocols to train and validate ML interatomic potentials are still in their infancy, and our simulated annealing runs did not yet unleash the full power of state-of-the-art global geometry optimization algorithms. Even so, a completely unexpected class of surface structures was readily identified for a well-studied type of

oxide crystals. That such simple structures have consistently eluded previous trial-structure-based surface structure determination work on IrO_2 or RuO_2 shows them to be counterintuitive, and one wonders how many more surprises await us when global geometry optimization based on predictive-quality machine-learned potentials has reached full maturity.

Supporting Information Available

See Supporting Information for additional detailed information on the reference database employed for the training of the ML potential and simulated annealing runs, on the *ab initio* thermodynamics results, on the initial-state core level shift calculations, as well as on the experimental growth and characterization work. This material is available free of charge via the Internet at http://pubs.acs.org.

ACKNOWLEDGEMENT

This research was supported by the Kopernikus/P2X programme (Cluster FC-A1) of the German Federal Ministry of Education and Research, the German Federal Environmental Foundation DBU and the German Academic Exchange Service DAAD. UD, MR and FK acknowledge support by the Austrian Science Fund (FWF, Z-250, Wittgenstein Prize). GSP acknowledges funding from the European Research Council (ERC) under the European Union's Horizon 2020 research and innovation program Grant agreement No. 864628. NR was supported by the Austrian Science Fund (FWF, Y847-N20, START Prize). ZQM acknowledges the support from the US National Science Foundation under grant DMR 1917579. We acknowledge fruitful discussions with Johannes Margraf and Simon Wengert. The authors thank Andreas Steiger-Thirsfeld (USTEM, TU Wien) for support with SEM measurements.

REFERENCES

(1) Kresse, G.; Bergermayer, W.; Podloucky, R.; Lundgren, E.; Koller, R.; Schmid, M.; Varga, P., Complex surface reconstructions solved by ab initio molecular dynamics. *Appl. Phys. A* **2003,** *76*, 701-710.

(2) Hussein, H. A.; Davis, J. B. A.; Johnston, R. L., DFT global optimisation of gas-phase and MgO-supported sub-nanometre AuPd clusters. *Phys. Chem. Chem. Phys.* **2016,** *18*, 26133-26143.

(3) Panosetti, C.; Krautgasser, K.; Palagin, D.; Reuter, K.; Maurer, R. J., Global Materials Structure Search with Chemically Motivated Coordinates. *Nano Lett.* **2015,** *15*, 8044-8048.

(4) Vilhelmsen, L. B.; Hammer, B., A genetic algorithm for first principles global structure optimization of supported nano structures. *J. Chem. Phys.* **2014,** *141*, 044711.

(5) Wexler, R. B.; Qiu, T.; Rappe, A. M., Automatic Prediction of Surface Phase Diagrams Using Ab Initio Grand Canonical Monte Carlo. *J. Phys. Chem. C* **2019,** *123*, 2321-2328.

(6) Wales, D. J.; Doye, J. P. K.; Miller, M. A.; Mortenson, P. N.; Walsh, T. R., Energy Landscapes: From Clusters to Biomolecules. *Adv. Chem. Phys.* **2000**, 1-111.

(7) Pintér, J. D., *Global Optimization: Scientific and Engineering Case Studies*. Springer US: New York, 2006; Vol. 85, p 546.

(8) Rupp, M.; von Lilienfeld, O. A.; Burke, K., Guest Editorial: Special Topic on Data-Enabled Theoretical Chemistry. *J. Chem. Phys.* **2018,** *148*, 241401.

(9) Behler, J., Perspective: Machine learning potentials for atomistic simulations. *J. Chem. Phys.* **2016,** *145*, 170901.

(10) Luo, J., Let thermodynamics do the interfacial engineering of batteries and solid electrolytes. *Energy Storage Mater.* **2019,** *21*, 50-60.

(11) Weiß, A.; Siebel, A.; Bernt, M.; Shen, T. H.; Tileli, V.; Gasteiger, H. A., Impact of Intermittent Operation on Lifetime and Performance of a PEM Water Electrolyzer. *J. Electrochem. Soc.* **2019,** *166*, F487-F497.

(12) Reier, T.; Teschner, D.; Lunkenbein, T.; Bergmann, A.; Selve, S.; Kraehnert, R.; Schlögl, R.; Strasser, P., Electrocatalytic Oxygen Evolution on Iridium Oxide: Uncovering Catalyst-Substrate Interactions and Active Iridium Oxide Species. *J. Electrochem. Soc.* **2014,** *161*, F876-F882.

(13) Bartók, A. P.; Payne, M. C.; Kondor, R.; Csányi, G., Gaussian Approximation Potentials: The Accuracy of Quantum Mechanics, without the Electrons. *Phys. Rev. Lett.* **2010,** *104*, 136403.

(14) Deringer, V. L.; Caro, M. A.; Csányi, G., Machine Learning Interatomic Potentials as Emerging Tools for Materials Science. *Adv. Mater.* **2019,** *31*, 1902765.

(15) Reuter, K., Ab Initio Thermodynamics and First-Principles Microkinetics for Surface Catalysis. *Catal. Lett.* **2016,** *146*, 541-563.

(16) McDaniel, C. L.; Schneider, S. J., Phase Relations in the Ru-lr-O(2) System in Air. *J. Res. Natl. Bur. Stand. A Phys. Chem.* **1969,** *73A*, 213-219.

(17) Liang, Z.; Li, T.; Kim, M.; Asthagiri, A.; Weaver, J. F., Low-temperature activation of methane on the IrO2 (110) surface. *Science* **2017,** *356*, 299.

(18) Abb, M. J. S.; Weber, T.; Glatthaar, L.; Over, H., Growth of Ultrathin Single-Crystalline IrO2(110) Films on a TiO2(110) Single Crystal. *Langmuir* **2019,** *35*, 7720-7726.

(19) Lee, Y.; Suntivich, J.; May, K. J.; Perry, E. E.; Shao-Horn, Y., Synthesis and Activities of Rutile IrO2 and RuO2 Nanoparticles for Oxygen Evolution in Acid and Alkaline Solutions. *J. Phys. Chem. Lett.* **2012,** *3*, 399-404.

(20) Zeng, X.; Dang, D.; Leng, L.; You, C.; Wang, G.; Zhu, C.; Liao, S., Doped reduced graphene oxide mounted with IrO2 nanoparticles shows significantly enhanced performance as a cathode catalyst for Li-O2 batteries. *Electrochim. Acta* **2016,** *192*, 431-438.
(21) Felix, C.; Bladergroen, J. B.; Linkov, V.; Pollet, G. B.; Pasupathi, S., Ex-Situ Electrochemical Characterization of IrO2 Synthesized by a Modified Adams Fusion Method for the Oxygen Evolution Reaction. *Catalysts* **2019,** *9*.
(22) Ryu, W.-H.; Lee, Y. W.; Nam, Y. S.; Youn, D.-Y.; Park, C. B.; Kim, I.-D., Crystalline IrO2-decorated TiO2 nanofiber scaffolds for robust and sustainable solar water oxidation. *J. Mater. Chem. A* **2014,** *2*, 5610-5615.
(23) Pai, W. W.; Wu, T. Y.; Lin, C. H.; Wang, B. X.; Huang, Y. S.; Chou, H. L., A cross-sectional scanning tunneling microscopy study of IrO2 rutile single crystals. *Surf. Sci.* **2007,** *601*, L69-L72.
(24) Anantharaj, S.; Karthik, P. E.; Kundu, S., Self-assembled IrO2 nanoparticles on a DNA scaffold with enhanced catalytic and oxygen evolution reaction (OER) activities. *J. Mater. Chem. A* **2015,** *3*, 24463-24478.
(25) Guo, K.; Li, Y.; Yuan, T.; Dong, X.; Li, X.; Yang, H., Ultrafine IrO2 nanoparticle-decorated carbon as an electrocatalyst for rechargeable Li–O2 batteries with enhanced charge performance and cyclability. *J. Solid State Electrochem.* **2015,** *19*, 821-829.
(26) Bartók, A. P.; Kondor, R.; Csányi, G., On representing chemical environments. *Phys. Rev. B* **2013,** *87*, 184115.
(27) Giannozzi, P.*, et al.*, QUANTUM ESPRESSO: A modular and open-source software project for quantum simulations of materials. *J. Phys.: Condens. Matter* **2009,** *21*, 395502.
(28) Hammer, B.; Hansen, L. B.; Nørskov, J. K., Improved adsorption energetics within density-functional theory using revised Perdew-Burke-Ernzerhof functionals. *Phys. Rev. B* **1999,** *59*, 7413-7421.
(29) Opalka, D.; Scheurer, C.; Reuter, K., Ab Initio Thermodynamics Insight into the Structural Evolution of Working IrO2 Catalysts in Proton-Exchange Membrane Electrolyzers. *ACS Catal.* **2019,** *9*, 4944-4950.
(30) Wang, T.; Jelic, J.; Rosenthal, D.; Reuter, K., Exploring Pretreatment–Morphology Relationships: Ab Initio Wulff Construction for RuO2 Nanoparticles under Oxidising Conditions. *ChemCatChem* **2013,** *5*, 3398-3403.
(31) Perdew, J. P.; Burke, K.; Ernzerhof, M., Generalized Gradient Approximation Made Simple. *Phys. Rev. Lett.* **1996,** *77*, 3865-3868.
(32) Dulub, O.; Valentin, C. D.; Selloni, A.; Diebold, U., Structure, defects, and impurities at the rutile TiO2(011)-(2×1) surface: A scanning tunneling microscopy study. *Surf. Sci.* **2006,** *600*, 4407-4417.
(33) Freakley, S. J.; Ruiz-Esquius, J.; Morgan, D. J., The X-ray photoelectron spectra of Ir, IrO2 and IrCl3 revisited. *Surf. Interface Anal.* **2017,** *49*, 794-799.
(34) Lundgren, E.; Kresse, G.; Klein, C.; Borg, M.; Andersen, J. N.; De Santis, M.; Gauthier, Y.; Konvicka, C.; Schmid, M.; Varga, P., Two-Dimensional Oxide on Pd(111). *Phys. Rev. Lett.* **2002,** *88*, 246103.
(35) Campbell, C. T., Transition Metal Oxides: Extra Thermodynamic Stability as Thin Films. *Phys. Rev. Lett.* **2006,** *96*, 066106.
(36) Reuter, K., Nanometer and Subnanometer Thin Oxide Films at Surfaces of Late Transition Metals. In *Nanocatalysis*, Heiz, U.; Landman, U., Eds. Springer Berlin Heidelberg: Berlin, Heidelberg, 2007; pp 343-376.

(37) Balajka, J.; Aschauer, U.; Mertens, S. F. L.; Selloni, A.; Schmid, M.; Diebold, U., Surface Structure of TiO2 Rutile (011) Exposed to Liquid Water. *J. Phys. Chem. C* **2017,** *121*, 26424-26431.